ChemComm

COMMUNICATION

View Article Online
View Journal | View Issue

Open Access Article. Published on 29 November 2018. Downloaded on 11/9/2025 9:11:07 AM.
This article is licensed under a Creative Commons Attribution 3.0 Unported Licence.

Check for updates

Cite this: *Chem. Commun.*, 2019, 55, 99

Received 9th November 2018,
Accepted 29th November 2018

DOI: 10.1039/c8cc08932a

rsc.li/chemcomm

Direct synthesis of MoS_2 or MoO_3 *via* thermolysis of a dialkyl dithiocarbamato molybdenum(IV) complex†

Niting Zeng,[a] David G. Hopkinson,[a] Ben F. Spencer,[a] Simon G. McAdams,[a] Aleksander A. Tedstone,[b] Sarah J. Haigh[a] and David J. Lewis*[a]

Direct synthesis of either 2H-MoS_2 or α-MoO_3 is made possible by thermolysis of the same single source precursor in either argon or air at moderate temperatures.

The inorganic compounds molybdenum disulphide (MoS_2) and molybdenum trioxide (MoO_3) have attracted significant attention. The 2H-MoS_2 polytype is an intrinsic semiconductor with a layered structure and has been extensively studied. Its promising applications include semiconductor technology,[1,2] catalysts[3,4] and energy storage.[5,6] Production of atomically thin MoS_2 as a complementary 2D material to graphene is also a widespread area of research. Atomically thin MoS_2 can be produced by micromechanical exfoliation,[7–9] liquid phase exfoliation,[10–13] chemical vapour deposition,[14–17] hydrothermal synthesis,[18,19] and hybrid chemical methods.[20,21] Similarly, α-MoO_3 also has a layered structure and exhibits excellent properties for charge-generation[22,23] and lithium ion storage[24,25] as well as catalytic properties.[26,27] For both materials, their properties are highly dependent on crystallite size and morphology, as well as the presence of surfactants. For example, MoO_3 thin films are used for charge generation, whilst MoO_3 nanorods or nanobelts are preferred for lithium storage. Nanocrystals are employed in catalysis.[23–27] Hence, controllable synthesis is of interest for both the facile design of crystalline MoO_3 and scalable production of atomically thin MoS_2.[8,22,28]

We have been interested in thin film deposition of MoS_2 by use of single source precursors. For example, tetrakis(*N*,*N*-diethyldithiocarbamato)molybdenum(IV) ($Mo(DTC)_4$, Scheme 1) can be used in combination with other metal dithiocarbamate complexes to produce doped MoS_2 *via* aerosol-assisted chemical vapour deposition (AACVD).[29] Molybdenum dithiocarbamate (MoDTC) has also been used as a lubricant additive which has been widely investigated for its decomposition mechanism to molybdenum sulfide species in tribology;[30,31] MoS_2 and MoO_3 are reported as two major products in tribological experiments, whilst another study recently revealed that MoS_2, $FeMoO_4$ and MoS_x (where $x > 2$) are the dominant species formed under certain conditions.[32]

Here we report the direct synthesis of either 2H-MoS_2 or α-MoO_3 from a single molecular precursor, with the reaction product controlled by choice of processing conditions. $Mo(DTC)_4$ was produced as per Lewis *et al.*[29] The growth of 2H-MoS_2 was achieved *via* thermolysis of $Mo(DTC)_4$ in argon whilst bulk α-MoO_3 was formed by the same reaction but in air. The characterisation performed shows that the 2H-MoS_2 powder produced is free-standing and nanostructured whilst polycrystalline α-MoO_3 is produced in air. The low temperature (450 °C) combined with the short processing time for both routes (1 h) represents a new soft synthetic pathway toward these important functional inorganic materials (Scheme 1).

Raman spectra (Fig. 1) indicate that the reaction under argon produces MoS_2 with the in-plane mode E^1_{2g} observed at 380 cm^{-1} and the out-of-plane mode A_{1g} located at 403 cm^{-1} ($\Delta\nu$ = 23 cm^{-1}).[9] The softening of the two modes together with the broadening of peaks may be caused by phonon confinement,[33] which suggested that the material was few-layer. For reaction in air, MoO_3 is formed with lattice modes below

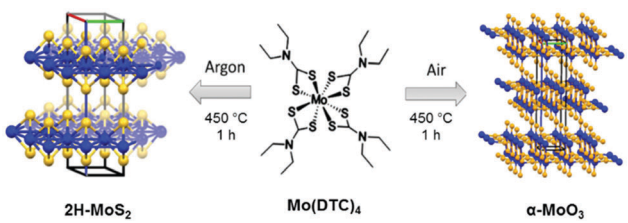

Scheme 1 Selective reaction for the solventless synthesis of molybdenum disulphide or molybdenum trioxide. MoS_2 was produced under argon while MoO_3 was formed in air; both reactions proceed from the same molecular precursor, $Mo(DTC)_4$. The reaction in both cases was carried out in a ceramic crucible placed within a tube furnace maintained at 450 °C for one hour only.

[a] School of Materials, University of Manchester, Oxford Road, M13 9PL, UK. E-mail: david.lewis-4@manchester.ac.uk
[b] School of Chemistry, University of Manchester, Oxford Road, M13 9PL, UK

† Electronic supplementary information (ESI) available. See DOI: 10.1039/c8cc08932a

Open Access Article. Published on 29 November 2018. Downloaded on 11/9/2025 9:11:07 AM.
This article is licensed under a Creative Commons Attribution 3.0 Unported Licence.

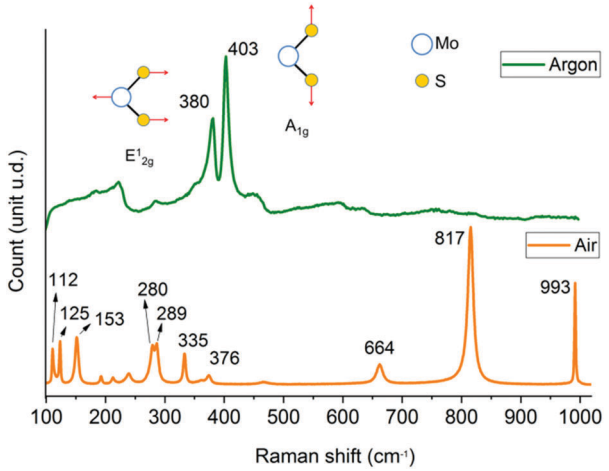

Fig. 1 Raman spectra of reaction products of thermolysis after one hour reaction at 450 °C under argon flow at 300 sccm with typical MoS_2 peaks at 380 cm^{-1} and 403 cm^{-1}; air environment with nine peaks that can all be assigned to α-MoO_3.

200 cm^{-1}, deformation modes between 450 cm^{-1} and 200 cm^{-1} and stretching modes above 450 cm^{-1}.[34] The peaks at 112 cm^{-1} (B_{2g}, B_{3g}), 125 cm^{-1} and 153 cm^{-1} (A_g, B_{1g}) represent vibrations of the main chains of Mo atoms, and the peaks at 280, 289 cm^{-1} (B_{2g}, B_{3g}) are assigned to the wagging vibrational mode of pendant oxygens.[35] The characteristic peaks at 664 cm^{-1} (B_{2g}, B_{3g}), 817 cm^{-1} (A_g, B_{1g}) and 993 cm^{-1} (A_g, B_{1g}) are associated with the symmetric and asymmetric stretching modes of α-MoO_3.[34–36]

X-ray powder diffraction (XRPD) was used to investigate the crystallographic structure of the materials produced. The diffraction pattern in argon is non-identical compared to standard 2H-MoS_2 (JCPDS No. 37-1492). Peaks corresponding to the (101) and (110) planes of MoS_2 are relatively intense whereas the peaks corresponding to the (002) and (103) planes are extremely broadened (Fig. 2). A preferred orientation in the (101) and (110) planes is evinced by the pattern, which suggests MoS_2 crystallites may grow laterally during the thermolysis process. The reflection of the (002) plane is very weak, indicating a reduced amount of bulk character in the [00*l*] direction.[37] This indicated again that potentially sheets of nanoscale thickness of MoS_2 were produced from this reaction pathway.[33,38,39] The XRPD diffraction pattern of the product of the decomposition of $Mo(DTC)_4$ in air at 450 °C matches well with orthorhombic α-MoO_3 (JCPDS No. 05-0508, Fig. 2). Strong intensities are noticed for the (110), (021) and (002) reflections, which indicates preferred growth orientations along these planes. No reflections assigned to MoO_2 or Mo_4O_{11} are observed, which indicates high-purity α-MoO_3 is formed in this reaction.

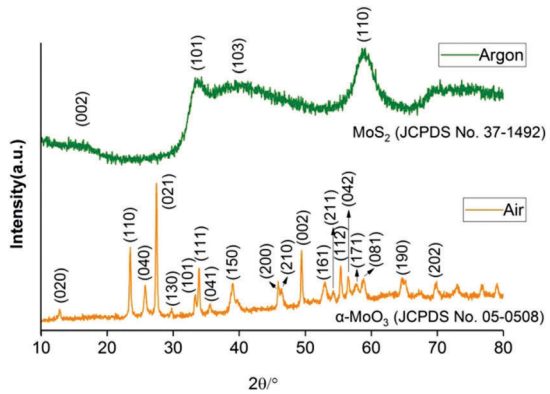

Fig. 2 XRPD patterns of products from reaction in argon (2H-MoS_2) and in air (α-MoO_3) with peaks indexed to 2H-MoS_2 (JCPDS 37-1492) and α-MoO_3 (JCPDS 05-0508) respectively.

X-ray photoelectron spectroscopy (XPS) was used to characterise the chemical information and changes occurring at the surface of the materials. A neutraliser was used to remove differential charging occurring to the powders under the X-ray beam, and binding energy scale calibration was performed using the C 1s photoelectron peak at 284.8 eV. The Mo 3d spectrum under argon (Fig. 3a) is fit with three chemical species with binding energies of 228.9, 230.0 and 232.5 eV and are associated with Mo^{4+} (MoS_2), Mo^{5+} and Mo^{6+} (MoO_3) respectively.[41,42] This is in good agreement with Raman results; MoS_2 is the dominant material formed from reaction under argon with oxidation occurring at the surface (sampling depth for Al Kα is *ca.* 6 nm). The Mo 3d spectrum also contains the broad S 2s photoelectron peak at 226.6 eV which is suggestive of the 2H-phase for MoS_2 consistent with diffraction results.[40] The S 2p spectrum also shows three chemical species, consistent with the Mo spectrum, with S $2p_{3/2}$ binding energy positions at 161.6, 162.8 and 168.4 eV (Fig. 3b), associated with S^{2-}, (MoS_2), S^{1-} and S^{6+} (sulfate) respectively, which are again consistent with MoS_2 reported in the literature and exhibiting some surface oxidation.[33,41,42] The ratio of Mo : S (excluding the oxidized species in the spectra, and adjusted to the relative sensitivity factor each elemental core level) is calculated as 1 : 2.1, indicating stoichiometric MoS_2.

For the reaction in air, the Mo 3d spectrum is adequately fit with one chemical species with a Mo $3d_{5/2}$ binding energy

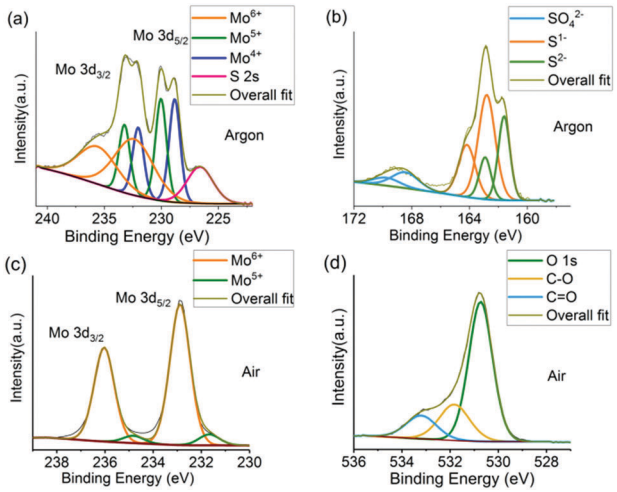

Fig. 3 High resolution XPS spectra. Mo 3d spectra for (a) product from reaction in argon and (b) product from reaction in air. (c) S 2p spectrum for product from reaction in argon. (d) O 1s peak for the product from reaction in air.

 This journal is © The Royal Society of Chemistry 2019

Open Access Article. Published on 29 November 2018. Downloaded on 11/9/2025 9:11:07 AM.
This article is licensed under a Creative Commons Attribution 3.0 Unported Licence.

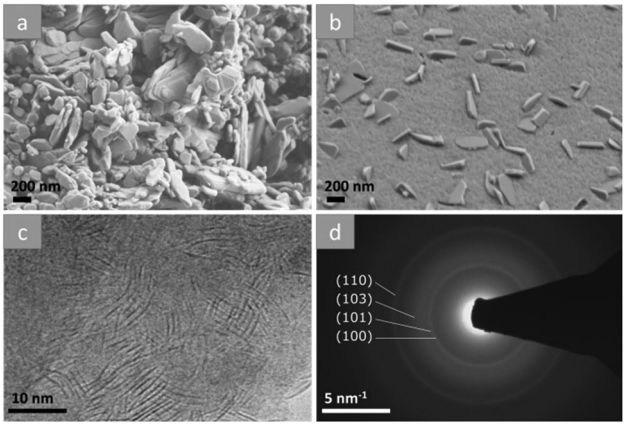

Fig. 4 Electron microscopy of thermolysis products. (a) SEM imaging after thermolysis at 450 °C in air and (b) in argon. (c & d) TEM image and SAED pattern for reaction products from argon. The SAED pattern is indexed to the diffraction pattern of 2H-MoS_2.

position of 232.9 eV (Fig. 3c), associated with Mo^{6+} (MoO_3).[43] This indicates the major oxidation state is (VI). No Mo^{4+} species are observed, and no signal from S is observed.

The O 1s peak with the largest contribution has a binding energy of 530.7 eV and is associated with metal oxide, with other species at ~532–534 eV associated with adventitious carbon oxide contamination. This is in agreement with prototypical MoO_3 reported in the literature.[43] The ratio of Mo : O (adjusted for relative sensitivity factors) is calculated as 1 : 2.80, indicating a stoichiometric oxide. This is also reflected by the relatively narrow full-width-at-half maximum for the Mo^{6+}, whereas this oxidized species in the MoS_2 (argon) sample is much broader indicating an array of partial oxide states (as expected for surface oxidation).

The materials were further investigated using electron microscopy. Scanning electron microscope (SEM) images of the product from reaction in argon shows evenly distributed large crystallites (Fig. 4(b)) of around 200–500 nm in length embedded in a nanostructured surface. Transmission electron microscopy (TEM) reveals that the textured surface is comprised of few-layer nanosheets (Fig. 4c), which must be the dominant species within the sample when taken into consideration together with the SEM images. Atomic force microscopy (AFM) of the powder dispersed by sonication in *N*-methyl-2-pyrrolidone and drop cast onto silicon substrates for analysis was used to confirm a mean flake thickness of ~10 nm (N = 83). Selected area electron diffraction (SAED) shows that these sheets give a polycrystalline diffraction pattern which was indexed to 2H-MoS_2 (Fig. 4d) in good agreement with XRPD results and as-expected for an ensemble of nanosheets with random orientations. SEM images show that the reaction products from air (Fig. 4a) appear to be tabular nanocrystallites with various sizes and shapes that are noticeably larger compared to the reaction products formed from argon atmospheres.

In this study, the solventless thermolysis of a single source precursor has been proven to be viable route to produce either 2H-MoS_2 or α-MoO_3 by judicious choice of reaction conditions. In argon, thin-layer MoS_2 nanosheets and nanoparticles are produced, which was confirmed by the broadening of both Raman peaks and XRPD reflections. XRPD further indicates very small polycrystalline sheets formed directly from the reaction which matches with both TEM and SAED results. Based on the thermogravimetric analysis (TGA) data published previously for $Mo(DTC)_4$ under argon the reaction proceeds by loss of the organic parts of the molecule as gaseous species to form amorphous MoS_x, followed by formation of crystalline 2H-MoS_2.[44] In air, these steps are probably followed by a rapid replacement of sulfur by atmospheric oxygen to form MoO_3, or by oxidation of the MoS_x intermediates to MoO_x species followed by formation of MoO_3.[44]

We conclude that the production of high-purity MoS_2 or MoO_3 is achievable by this method with potential scalability embedded. By using various combinations of precursors (of which for metal dithiocarbamates[45] and metal xanthates[46] there are many) we should be able to produce large amounts of doped metal oxide and chalcogenide materials for various applications including catalysis, tribology and dilute magnetic semiconductor materials for spintronics. As these are layered structures we might also be able to exfoliate them to the two-dimensional limit to produce bespoke metal oxide and chalcogenide 2D materials. We are currently exploring these possibilities in our laboratory. This approach has already proven to be successful for producing synthetic layered main group sulfides and 2D derivatives thereof.[47]

DJL and NZ would like to thank the University of Manchester Research Impact Donor Scholarship for funding this study. SGMcA is funded by an EPSRC doctoral prize. DGH is funded by the EPSRC Centre for Doctoral Training in the Science and Applications of Graphene and Related Nanomaterials (GrapheneNOWNANO, EP/L01548X/1).

Conflicts of interest

There are no conflicts to declare.

Notes and references

1 G. Fiori, F. Bonaccorso, G. Iannaccone, T. Palacios, D. Neumaier, A. Seabaugh, S. K. Banerjee and L. Colombo, *Nat. Nanotechnol.*, 2014, **9**, 768.
2 A. Splendiani, L. Sun, Y. Zhang, T. Li, J. Kim, C.-Y. Chim, G. Galli and F. Wang, *Nano Lett.*, 2010, **10**, 1271–1275.
3 Y. Li, H. Wang, L. Xie, Y. Liang, G. Hong and H. Dai, *J. Am. Chem. Soc.*, 2011, **133**, 7296–7299.
4 P. Raybaud, J. Hafner, G. Kresse, S. Kasztelan and H. Toulhoat, *J. Catal.*, 2000, **190**, 128–143.
5 X. Y. Yu, H. Hu, Y. Wang, H. Chen and X. W. Lou, *Angew. Chem., Int. Ed.*, 2015, **54**, 7395–7398.
6 K. Chang, D. Geng, X. Li, J. Yang, Y. Tang, M. Cai, R. Li and X. Sun, *Adv. Energy Mater.*, 2013, **3**, 839–844.
7 K. F. Mak, C. Lee, J. Hone, J. Shan and T. F. Heinz, *Phys. Rev. Lett.*, 2010, **105**, 136805.
8 K. S. Novoselov, D. Jiang, F. Schedin, T. J. Booth, V. V. Khotkevich, S. V. Morozov and A. K. Geim, *Proc. Natl. Acad. Sci. U. S. A.*, 2005, **102**, 10451–10453.
9 C. Lee, H. Yan, L. E. Brus, T. F. Heinz, J. Hone and S. Ryu, *ACS Nano*, 2010, **4**, 2695–2700.
10 J. N. Coleman, M. Lotya, A. O'Neill, S. D. Bergin, P. J. King, U. Khan, K. Young, A. Gaucher, S. De, R. J. Smith, I. V. Shvets, S. K. Arora, G. Stanton, H. Y. Kim, K. Lee, G. T. Kim, G. Duesberg, T. Hallam,

Open Access Article. Published on 29 November 2018. Downloaded on 11/9/2025 9:11:07 AM.
This article is licensed under a Creative Commons Attribution 3.0 Unported Licence.

J. J. Boland, J. J. Wang, J. F. Donegan, J. C. Grunlan, G. Moriarty, A. Shmeliov, R. J. Nicholls, J. M. Perkins, E. M. Grieveson, K. Theuwissen, D. W. McComb, P. D. Nellist and V. Nicolosi, *Science*, 2011, **331**, 568–571.
11 G. S. Bang, K. W. Nam, J. Y. Kim, J. Shin, J. W. Choi and S.-Y. Choi, *ACS Appl. Mater. Interfaces*, 2014, **6**, 7084–7089.
12 K. Wang, J. Wang, J. Fan, M. Lotya, A. O'Neill, D. Fox, Y. Feng, X. Zhang, B. Jiang, Q. Zhao, H. Zhang, J. N. Coleman, L. Zhang and W. J. Blau, *ACS Nano*, 2013, **7**, 9260–9267.
13 A. Jawaid, D. Nepal, K. Park, M. Jespersen, A. Qualley, P. Mirau, L. F. Drummy and R. A. Vaia, *Chem. Mater.*, 2016, **28**, 337–348.
14 B. Liu, L. Chen, G. Liu, A. N. Abbas, M. Fathi and C. Zhou, *ACS Nano*, 2014, **8**, 5304–5314.
15 M. R. Laskar, L. Ma, S. Kannappan, P. S. Park, S. Krishnamoorthy, D. N. Nath, W. Lu, Y. Wu and S. Rajan, *Appl. Phys. Lett.*, 2013, **102**, 252108.
16 X. Wang, H. Feng, Y. Wu and L. Jiao, *J. Am. Chem. Soc.*, 2013, **135**, 5304–5307.
17 Y. Zhan, Z. Liu, S. Najmaei, P. M. Ajayan and J. Lou, *Small*, 2012, **8**, 966–971.
18 D. Wang, Z. Pan, Z. Wu, Z. Wang and Z. Liu, *J. Power Sources*, 2014, **264**, 229–234.
19 K. Krishnamoorthy, G. K. Veerasubramani, S. Radhakrishnan and S. J. Kim, *Mater. Res. Bull.*, 2014, **50**, 499–502.
20 H. Samassekou, A. Alkabsh, M. Wasala, M. Eaton, A. Walber, A. Walker, O. Pitkänen, K. Kordas, S. Talapatra, T. Jayasekera and D. Mazumdar, *2D Mater.*, 2017, **4**, 021002.
21 T. Sreeprasad, P. Nguyen, N. Kim and V. Berry, *Nano Lett.*, 2013, **13**, 4434–4441.
22 J. Meyer, S. Hamwi, M. Kröger, W. Kowalsky, T. Riedl and A. Kahn, *Adv. Mater.*, 2012, **24**, 5408–5427.
23 H. Kanno, R. J. Holmes, Y. Sun, S. Kena-Cohen and S. R. Forrest, *Adv. Mater.*, 2006, **18**, 339–342.
24 Z. Wang, S. Madhavi and X. W. Lou, *J. Phys. Chem. C*, 2012, **116**, 12508–12513.
25 J. S. Chen, Y. L. Cheah, S. Madhavi and X. W. Lou, *J. Phys. Chem. C*, 2010, **114**, 8675–8678.
26 M. A. Vuurman and I. E. Wachs, *J. Phys. Chem.*, 1992, **96**, 5008–5016.
27 A. Manivel, G.-J. Lee, C.-Y. Chen, J.-H. Chen, S.-H. Ma, T.-L. Horng and J. J. Wu, *Mater. Res. Bull.*, 2015, **62**, 184–191.
28 S. Balendhran, S. Walia, H. Nili, J. Z. Ou, S. Zhuiykov, R. B. Kaner, S. Sriram, M. Bhaskaran and K. Kalantar-zadeh, *Adv. Funct. Mater.*, 2013, **23**, 3952–3970.
29 D. J. Lewis, A. A. Tedstone, X. L. Zhong, E. A. Lewis, A. Rooney, N. Savjani, J. R. Brent, S. J. Haigh, M. G. Burke, C. A. Muryn, J. M. Raftery, C. Warrens, K. West, S. Gaemers and P. O'Brien, *Chem. Mater.*, 2015, **27**, 1367–1374.
30 C. Grossiord, K. Varlot, J.-M. Martin, T. Le Mogne, C. Esnouf and K. Inoue, *Tribol. Lett.*, 1998, **31**, 737–743.
31 M. I. de Barros' Bouchet, J. M. Martin, T. Le-Mogne and B. Vacher, *Tribol. Lett.*, 2005, **38**, 257–264.
32 D. N. Khaemba, A. Neville and A. Morina, *RSC Adv.*, 2016, **6**, 38637–38646.
33 C. N. R. Rao and A. Nag, *Eur. J. Inorg. Chem.*, 2010, 4244–4250.
34 L. Seguin, M. Figlarz, R. Cavagnat and J.-C. Lassègues, *Spectrochim. Acta, Part A*, 1995, **51**, 1323–1344.
35 B. C. Windom, W. Sawyer and D. W. Hahn, *Tribol. Lett.*, 2011, **42**, 301–310.
36 M. A. Py and K. Maschke, *Physica B+C*, 1981, **105**, 370–374.
37 T. S. Sahu and S. Mitra, *Sci. Rep.*, 2015, **5**, 12571.
38 H. Ramakrishna Matte, A. Gomathi, A. K. Manna, D. J. Late, R. Datta, S. K. Pati and C. Rao, *Angew. Chem., Int. Ed.*, 2010, **49**, 4059–4062.
39 G. L. Frey, R. Tenne, M. J. Matthews, M. Dresselhaus and G. Dresselhaus, *Phys. Rev. B: Condens. Matter Mater. Phys.*, 1999, **60**, 2883.
40 H. W. Wang, P. Skeldon and G. Thompson, *Surf. Coat. Technol.*, 1997, **91**, 200–207.
41 K.-K. Liu, W. Zhang, Y.-H. Lee, Y.-C. Lin, M.-T. Chang, C.-Y. Su, C.-S. Chang, H. Li, Y. Shi, H. Zhang, C.-S. Lai and L.-J. Li, *Nano Lett.*, 2012, **12**, 1538–1544.
42 M. A. Baker, R. Gilmore, C. Lenardi and W. Gissler, *Appl. Surf. Sci.*, 1999, **150**, 255–262.
43 D. O. Scanlon, G. W. Watson, D. J. Payne, G. R. Atkinson, R. G. Egdell and D. S. L. Law, *J. Phys. Chem. C*, 2010, **114**, 4636–4645.
44 M. N. McCain, B. He, J. Sanati, Q. J. Wang and T. J. Marks, *Chem. Mater.*, 2008, **20**, 5438–5443.
45 G. Hogarth, *Progress in Inorganic Chemistry*, John Wiley & Sons, 2005.
46 E. R. T. Tiekink and G. Winter, *Rev. Inorg. Chem.*, 1992, **12**, 183.
47 K. Norton, J. Kunstmann, L. Ping, A. Rakowski, C. Wang, A. J. Marsden, G. Murtuza, N. Zeng, S. McAdams, M. A. Bissett, S. J. Haigh, B. Derby, G. Seifert and D. J. Lewis, *Chem. Sci.*, 2019, DOI: 10.1039/C1038SC04018D.

 This journal is © The Royal Society of Chemistry 2019